Simulation of phonon transport across a non-polar nanowire junction using an atomistic Green's function method

W. Zhang,[1] N. Mingo,[2] and T. S. Fisher[1,*]
[1]*Nanoscale Thermo-Fluids Laboratory, Birck Nanotechnology Center, Purdue University, West Lafayette, Indiana 47907, USA*
[2]*NASA-Ames Center for Nanotechnology, 229-1, Moffett Field, California 94035, USA*
(Received 19 January 2007; published 19 November 2007)

Phonon transport across a non-polar nanowire situated between two semi-infinite contacts is simulated in this paper using the atomistic Green's function method. Abrupt geometric changes between the nanowire and bulk contacts are handled by self-energy matrices obtained from bare surface Green's functions. Transport properties such as phonon transmission functions and thermal conductances are calculated, and their dependencies on the interatomic potential, length, diameter, shape, and lattice orientation are investigated. The results reveal that the overall thermal conductance of the nanowire–bulk-contact structure increases with nanowire diameter while the normalized thermal conductance approaches an asymptotic value. Thermal conductance decreases significantly with increasing nanowire length and converges to that of the single-contact case. This method can be generalized to study phonon transport through a variety of nanostructures between bulk contacts.

DOI: 10.1103/PhysRevB.76.195429 PACS number(s): 68.65.La, 63.22.+m, 66.70.+f

I. INTRODUCTION

The trend toward smaller semiconductor devices and material characteristics at nanometer scales offers new opportunities and challenges in characterizing phonon transport. New fabrication processes have emerged to control device geometries with almost atomic precision, such as suspended silicon nanowires with lateral dimensions as small as 40 nm.[1] With these advances, new experimental techniques have been developed in recent years to measure the thermal and electrical properties of nanostructures,[2,3] and new numerical tools have been developed to understand selected transport phenomena.[4] As a building block of low-dimensional micro-/nanodevices, nanowires have received considerable attention in recent years owing to their unique thermal, electrical, and optical properties.[5] This paper employs an atomistic Green's function method to simulate phonon transport through a non-polar nanowire between bulk contacts.

Thermal transport in nanostructures has been simulated with a variety of numerical methods. One class of approaches treats phonons as particles[6] whose motion is described by the Boltzmann transport equation (BTE). Jiaung and Ho[7] used a lattice Boltzmann method to solve the phonon BTE with relaxation time assumptions. They studied size effects in bended and straight nanoducts by treating boundary scattering with a specularity parameter. They assumed that all phonons relax to the equilibrium Bose-Einstein distribution after collisions and concluded that geometric effects depend strongly on the Knudsen number. Chen *et al.*[8] used a Monte Carlo method to calculate the thermal conductivity of a silicon nanowire. They developed a genetic algorithm to handle three-phonon scattering processes and showed that thermal conductivity decreases as the diameter decreases.

The thermal conductivity of nanowires has also been modeled using the theory developed by Callaway[9] and Holland.[10] Huang *et al.*[11] investigated boundary scattering effects on the thermal conductivity of a hollow silicon nanowire. They obtained phonon dispersion curves and average phonon group velocity from elasticity equations. They then used the Callaway formula to calculate the thermal conductivity. Mingo[12] used full phonon dispersion curves, obtained from atomic-scale dynamic equations and appropriate interatomic potentials, to calculate the thermal conductivity of silicon nanowire, and the numerical results exhibited good agreement with experimental data.[13]

Another major class of thermal models of nanowires focuses on ballistic transport properties and emphasizes the effects of bulk contacts on nanowire transport. Similar effects have been documented well in ballistic electron transport studies.[14] For the abrupt junction between a semi-infinite cylindrical quantum wire and a three-dimensional bulk insulator, a recent publication by Chang and Geller[15] extends the perturbation method from the earlier two-dimensional thin plate work of Cross and Lifshitz[16] to calculate the transmission function for the four acoustic phonon branches using isotropic elasticity theory. They concluded that in the dominant longitudinal phonon branch, phonon transmission vanishes as ω^2 in the low-frequency limit and thermal conductance scales as T^3 at low temperatures.

Nanowire–bulk-contact transport falls into a larger category of point-contact problems, which are defined as microscopic regions of short links between bulk contacts that alter the dominant kinetic phenomena as compared to similar processes in bulk materials. Understanding transport in this type of structure provides significant insights into many other applications. For example, heat flow across two contacts can be studied as the collective result of transport through a number of parallel contacts. Low-temperature phonon transport in these structures has been recently reviewed by Feher *et al.*[17] The transport exhibits different types of ballistic features, and the energy flux is generally limited by weakly coupled short links such as nanowires, defects, and heterogeneous interfaces. Patton and Geller[18] presented a simple analytical formula (valid below 10 K) to predict the thermal conduc-

tance of a mesoscopic weak link, and they also proposed a scanning thermal probe made of a weak link between bulk contacts to detect the surface vibrational density of states.

Phonon engineering, i.e., tuning phonon spectra to engineer transport properties, has been proposed based on structure-related vibrational properties. One way to modify phonon spectra is by surface coating. Pokatilov *et al.*[19] theoretically investigated the effect of a heterogeneous coating on the acoustic phonon properties of semiconductor nanowires and predicted a substantial redistribution of elastic deformations and significant changes in thermal conduction. Their methods are based on elasticity theory and the assumption of an infinitely long nanowire. Later, their method was applied to GaN nanowires with AlN barriers.[20] Mingo and Yang[21] used the atomistic Green's function (AGF) method to investigate the effect of oxide coating on an infinitely long silicon nanowire. They observed a ballistic-diffusive transport transition in the phonon transmission function and demonstrated the significance of the bond strength between the nanowire and its coating. However, their work is again based on an infinitely long nanowire while, in practice, nanowires are usually connected to bulk contacts at a junction.

Buldum *et al.*[22] studied phonon transport through an infinitely long atomic wire and a finite atomic wire using a model Hamiltonian approach. They predicted stepwise behavior in ballistic thermal conductance for a uniform atomic chain at very low temperatures. They also found that resonant modes originating from longitudinal optical modes can contribute to ballistic thermal conductance and can induce stepwise behavior in the conductance. Li *et al.*[23] investigated ballistic phonon transmission through a rectangular superlattice nanowire between two semi-infinite blocks while considering only the longitudinal phonon mode.

Most prior work on nanowire phonon transport is based on acoustic theory and therefore lacks atomic-scale fidelity. High-frequency phonons and optical phonons are difficult to handle with acoustic theory. In addition, the abrupt geometry change between bulk contacts and nanowires is not always considered.[24] A comprehensive simulation should consider all phonon branches existing in nanowires and their coupling to phonon modes existing in the bulk contacts. The AGF method has been developed to handle full-spectrum ballistic phonon transport in non-polar nanostructures. It offers the flexibility to incorporate complicated geometries and material compositions, as well as atomic-scale fidelity. The major limitation of this method is the underlying harmonic assumption. A recent publication by Mingo[25] introduces a theoretical framework to include anharmonic effects. Another limitation of the method is the fact that the lattice coordination is fixed from the beginning, so that no atomic reorganization is allowed. Thus, the approach cannot be applied to systems where atomic diffusion or convection processes take place. The next sections of this paper describe the theory and implementation of the AGF method, followed by a section containing the results and related discussion.

II. PROBLEM DEFINITION AND THEORY

Solving a thermal transport problem with the atomic Green's function method involves several steps. First, harmonic matrices for the system and its components are generated to establish the harmonic relationship between any 2 atomic degrees of freedom. This step uses equilibrium atomic positions and a prescribed interatomic potential energy model. Then, Green's functions of the system and its components are calculated from the harmonic matrices. Although the definition of a Green's function is straightforward, an efficient algorithm can significantly reduce computation time and simplify numerical implementation. Thereafter, the frequency-dependent phonon transmission function is generated, and integration is performed over the full frequency spectrum for specified contact temperatures to calculate the net heat flow rate. The detailed description of the related theory and algorithmic details can be found in Refs. 21, 26, and 27.

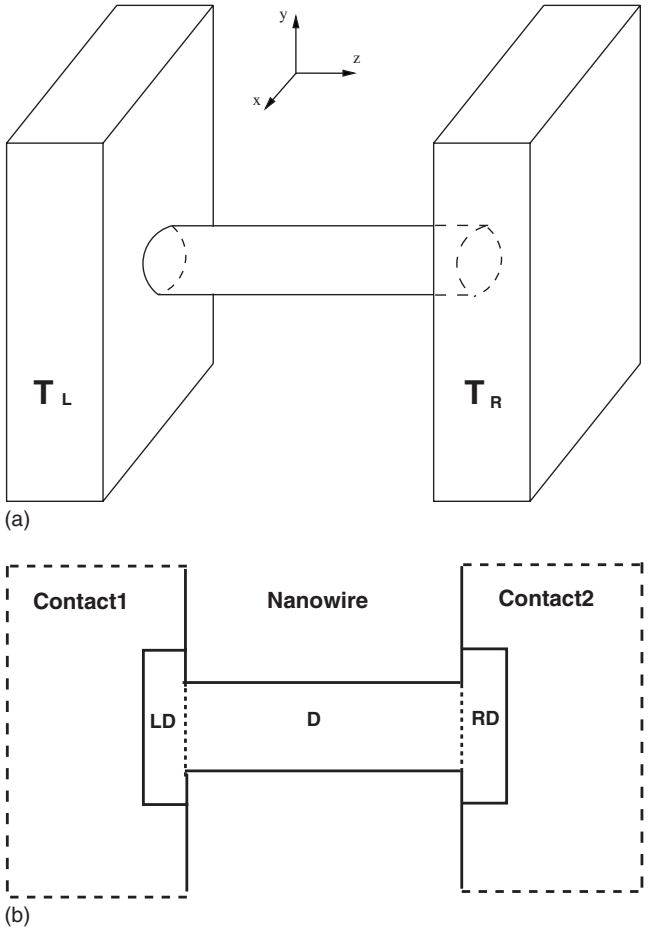

FIG. 1. Schematic diagram of a nanowire device between two bulk contacts. (a) 3D view. (b) 2D view with definitions of LD, D, and RD regions.

A model configuration of a nanowire between two semi-infinite contacts is shown in Fig. 1. A silicon nanowire bridges two bulk silicon contacts, "Contact1" and "Contact2," and its axis is aligned with the z direction. The connections between the nanowire and contacts are lattice valence bonds. The left bulk contact has a constant temperature of T_L and the right bulk contact has a constant temperature of T_R. Several groups of atoms are defined and shown in Fig. 1(b) for convenient reference in later sections. The "LD"

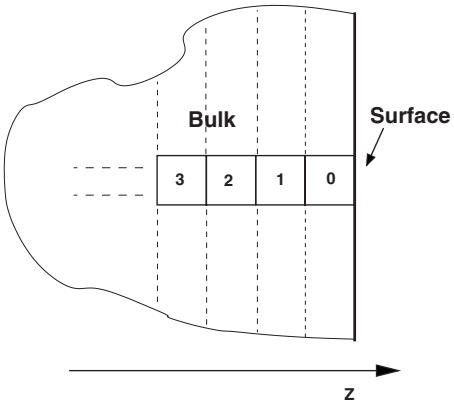

FIG. 2. Schematic diagram of a bare surface and bulk contact layers.

region contains those atoms that are in the left bulk contact and bond with nanowire atoms. The "RD" region contains atoms that are in the right bulk contact and bond with nanowire atoms. The "D" region includes all nanowire atoms and all atoms in LD and RD. For simplicity, atoms on the exposed surface of silicon are assumed to maintain their bulk lattice positions without any surface reconstruction.

A. Harmonic matrices and interatomic potentials

In the atomistic Green's function method, atom groups and their interactions can be represented by corresponding harmonic matrices defined as

$$\mathbf{H} = \{H_{pq}\} = \frac{1}{\sqrt{M_p M_q}} \begin{cases} -\dfrac{\partial^2 U}{\partial u_p \partial u_q} & \text{if } p \neq q \\ -\displaystyle\sum_{m \neq q} \dfrac{\partial^2 U}{\partial u_q \partial u_m} & \text{if } p = q, \end{cases} \tag{1}$$

where u_p and u_q refer to any two atomic vibrational degrees of freedom (i.e., displacements), respectively, and m is the running index. U represents the total interatomic potential. M_p and M_q are atomic masses associated with degrees of freedom u_p and u_q, respectively. A Stillinger-Weber (SW) potential is selected to approximate the interatomic potential U in silicon with pair and triplet contributions.[28] The SW potential has been popularly used to study phonon transport in Si lattices.[22,29] The ideal tetrahedral angle and diamond lattice are explicitly favored at equilibrium using this potential.

B. Bare surface Green's function

A semi-infinite bulk contact can be treated as an infinite stack of thin-film layers, and each thin-film layer can be represented by a unit cell with a plane wave formulation established in prior work[26] to take advantage of symmetry in the in-plane direction. This concept is shown in Fig. 2. Layer "0" is the surface layer whose right-hand neighboring layer does not exist. Layers "1," "2," and "3" are bulk layers with both left-hand and right-hand neighboring layers.

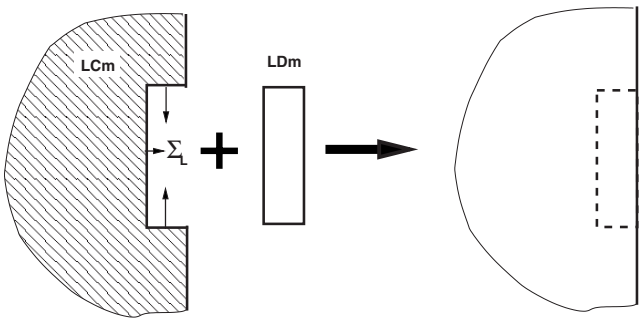

FIG. 3. Schematic diagram showing the assembly of regions required for the calculation of Σ_L.

The bulk Green's function of the left contact $(\mathbf{g}_{\mathrm{LCB}}(\omega, \vec{\mathbf{k}}_\parallel))$ is defined as

$$\mathbf{g}_{\mathrm{LCB}}(\omega, \vec{\mathbf{k}}_\parallel) \equiv \lim_{\delta \to 0} [(\omega^2 + \delta i)\mathbf{I} - \mathbf{H}_{\mathrm{LCB}}(\vec{\mathbf{k}}_\parallel)]^{-1}, \tag{2}$$

where ω is the phonon angular frequency and $\vec{\mathbf{k}}_\parallel$ is the parallel wave vector on the xy plane. $\mathbf{H}_{\mathrm{LCB}}(\vec{\mathbf{k}}_\parallel)$ is the "intralayer" matrix defined previously[26] that represents the harmonic behavior of the overall left bulk contact as a function of the parallel wave vector $\vec{\mathbf{k}}_\parallel$. δ is a small perturbation whose role is elaborated by Datta.[30,31] We note that the number of atoms in region "LCB" precludes any practical matrix inversion for Eq. (2). Fortunately, only a small part of $\mathbf{g}_{\mathrm{LCB}}$ is needed, i.e., the bulk Green's function associated with layer 1 $(\mathbf{g}_1)$. The decimation technique has been adopted to evaluate the Green's function $(\mathbf{g}_1)$ numerically because of its rapid convergence and low memory requirements.[32]

The bare surface Green's function $(\mathbf{g}_0(\omega, \vec{\mathbf{k}}_\parallel))$ can then be obtained as

$$\mathbf{g}_0(\omega, \vec{\mathbf{k}}_\parallel) \equiv \lim_{\delta \to 0} [(\omega^2 + \delta i)\mathbf{I} - \mathbf{H}_0(\vec{\mathbf{k}}_\parallel) - \tau_{0,1}\mathbf{g}_1\tau_{1,0}]^{-1}, \tag{3}$$

where $\tau_{0,1}$ and $\tau_{1,0}$ are interlayer matrices that link layers 1 and 0 $(\tau_{0,1} = \tau_{1,0}^\dagger)$. $\mathbf{H}_0(\vec{\mathbf{k}}_\parallel)$ is the intralayer matrix of layer 0. Note that $\mathbf{H}_0$ differs from $\mathbf{H}_1$ because layer 0 does not have a right-hand neighboring layer. A more detailed definition of "inter-layer" and intra-layer matrices can be found in Ref. 26.

C. Assembled surface Green's function $\tilde{g}_o$

The bare surface Green's function $\mathbf{g}_0$ obtained in the previous section is projected on one unit cell, and thus it is a 6×6 matrix because there are 6 degrees of freedom in a diamond structure unit cell. This method also applies to crystal structures with different numbers of degrees of freedom. However, a nanowire can have a cross section larger than that of one unit cell, and therefore, the interfacial area between bulk contacts and the nanowire can be larger than one unit cell. To construct surface Green's function of a multi-unit-cell interface, the Green's function $\tilde{g}_o$ must be assembled to be the same size as $\mathbf{H}_{\mathrm{LDm}}$, which is the harmonic matrix for atom group "LDm" (shown in Fig. 3). The atomic structure of "LDm" is identical to that of LD. The only dif-

ference is that LDm has no neighboring atoms to its right while LD is linked to the nanowire on its right side. Therefore, the harmonic matrices representing these two atom groups differ. The LDm region is employed solely to calculate the surface Green's function of the contact. We later show how this Green's function ($\tilde{g}_o$) is used to calculate self-energy matrices for a nanowire–bulk-contact structure.

Assuming that LDm contains n_{ld} degrees of freedom and thus $n_{uc,ld}(=n_{ld}/6)$ unit cells, $\tilde{g}_o$ must be an $n_{ld}\times n_{ld}$ matrix. The surface Green's function of the whole LDm region can be defined as

$$\hat{g}_o(\omega,\vec{k}_\parallel) = \begin{bmatrix} g_0 & \cdots & g_0 e^{-i\vec{k}_\parallel\cdot(\vec{R}_1-\vec{R}_{n_{uc,ld}})} \\ \vdots & g_0 e^{-i\vec{k}_\parallel\cdot(\vec{R}_v-\vec{R}_w)} & \vdots \\ g_0 e^{-i\vec{k}_\parallel\cdot(\vec{R}_{n_{uc,ld}}-\vec{R}_1)} & \cdots & g_0 \end{bmatrix}, \tag{4}$$

where v and w are index numbers for unit cells in LDm and both range from 1 to $n_{uc,ld}$. R_v and R_w are position vectors for unit cells v and w, respectively. In addition, an integration over $\vec{k}_\parallel$ is necessary to capture the effects of phonon waves from bulk contacts to the nanowire:

$$\tilde{g}_o(\omega) = \frac{1}{N^2}\sum_{\vec{k}_\parallel} \hat{g}_o(\omega,\vec{k}_\parallel), \tag{5}$$

where N^2 is the total number of discrete points in the $\vec{k}_\parallel$ space and is defined in prior work.[26]

D. Self-energy matrices

Self-energy matrices are needed to evaluate the device Green's function. The method to calculate self-energy matrices in this particular case differs from those of the thin-film[26] and atomic chain[27] cases, mainly because of the size mismatch at the interfaces between the nanowire and bulk contacts. Figure 3 illustrates the approach adopted here to calculate self-energy matrices.

Region "LCm" is defined as the left semi-infinite contact after removing atoms in LDm and is shown as the patterned area in Fig. 3. Physically, if the region LDm is added to the region LCm, then an uncoupled semi-infinite contact with a smooth and flat bare surface will be created. This process can be described in terms of the Green's function:

$$\tilde{g}_o = (\omega^2\mathbf{I} - \mathbf{H}_{\mathrm{LDm}} - \Sigma_L)^{-1}, \tag{6}$$

where $\tilde{g}_o$ is the Green's function for the atoms on a flat bare surface, and its calculation was previously described. $\mathbf{H}_{\mathrm{LDm}}$ is the harmonic matrix for region LDm. Σ_L represents the coupling of LCm to LDm (shown as small arrows in Fig. 3). The same self-energy matrix can be used to represent the coupling from LCm to LD as long as the harmonic matrix connecting the region LCm and the nanowire is a null matrix, i.e., no direct connection between LCm and the nanowire exists. Therefore, we can invert Eq. (6) to calculate Σ_L:

$$\Sigma_L = \omega^2\mathbf{I} - \mathbf{H}_{\mathrm{LDm}} - \tilde{g}_o^{-1}. \tag{7}$$

This is a crucial procedure that allows us to handle dimensional mismatches between a nanowire and semi-infinite contacts. Σ_R, which is the self-energy matrix of the right contact, can be obtained in the same way.

E. Nanowire Green's function

The nanowire Green's function can be expressed as

$$\mathbf{G} = (\omega^2\mathbf{I} - \mathbf{H}_D - \Sigma_L^d - \Sigma_R^d)^{-1}, \tag{8}$$

where $\mathbf{H}_D$ is the harmonic matrix of the D region. Σ_L^d and Σ_R^d are based on Σ_L and Σ_R:

$$\mathbf{\Sigma}_L^d \equiv \begin{bmatrix} \mathbf{\Sigma}_L & 0 & 0 \\ 0 & 0 & 0 \\ 0 & 0 & 0 \end{bmatrix}, \tag{9}$$

$$\mathbf{\Sigma}_R^d \equiv \begin{bmatrix} 0 & 0 & 0 \\ 0 & 0 & 0 \\ 0 & 0 & \mathbf{\Sigma}_R \end{bmatrix}. \tag{10}$$

The top left block of $\mathbf{\Sigma}_L^d$ contains Σ_L, and all other entries are zero to match the size of $\mathbf{H}_D$; similarly, the bottom right block of $\mathbf{\Sigma}_R^d$ contains Σ_R, and other entries are zero.

F. Transmission and heat flux

With Σ_L^d, Σ_R^d, and $\mathbf{G}$ calculated, one can easily obtain the transmission function Ξ:[27]

$$\Xi(\omega) = \mathrm{Tr}[\mathbf{\Gamma}_L\mathbf{G}\mathbf{\Gamma}_R\mathbf{G}^\dagger], \tag{11}$$

where $\mathbf{\Gamma}_L$ and $\mathbf{\Gamma}_R$ are defined as

$$\mathbf{\Gamma}_L(\omega) \equiv i(\Sigma_L^d - (\Sigma_L^d)^\dagger), \tag{12}$$

$$\mathbf{\Gamma}_R(\omega) \equiv i(\Sigma_R^d - (\Sigma_R^d)^\dagger). \tag{13}$$

Heat flux can then be calculated as

$$J = \int \frac{\hbar\omega}{2\pi}\Xi(\omega)(\bar{N}_L(\omega) - \bar{N}_R(\omega))d\omega, \tag{14}$$

where $\bar{N}_L$ and $\bar{N}_R$ are phonon distribution functions in the left and right contacts.

III. NUMERICAL IMPLEMENTATION

The plane wave formulation requires a mesh to discretize the first Brillouin zone (or its equivalent) in $\vec{\mathbf{k}}_\parallel$ space. The direct lattice, the reciprocal lattice and the first Brillouin zone, and the equivalent Brillouin zones for orientations (100) and (111) are shown in Fig. 4. Equivalent Brillouin zones are used to simplify the meshing process and are based on the concept of translational invariance in $\vec{k}_\parallel$ space. The overall dimension of the equivalent Brillouin zone used in our computations is shown as the patterned area in Fig. 4 and spans $\{k_x\in[0,2\sqrt{2}\pi/a), k_y\in[0,2\sqrt{2}\pi/a)\}$ for the (100) di-

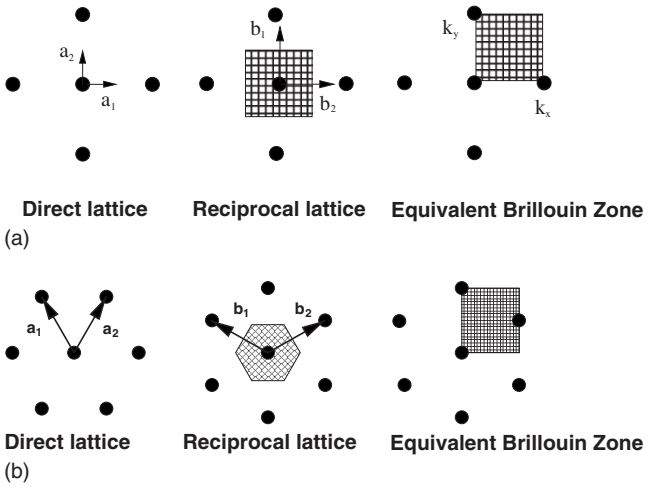

FIG. 4. Direct lattice, reciprocal lattice, first Brillouin zone, and equivalent Brillouin zone used in computations. (a) Silicon (100). (b) Silicon (111).

rection and $\{k_x \in [0, 2\sqrt{2}\pi/a), k_y \in [0, 4\sqrt{6}\pi/3a)\}$ for the (111) direction, where a is the lattice constant of silicon. A 430×430 mesh for the (100) orientation and a 400×461 mesh for the (111) orientation are used to discretize these equivalent Brillouin zones. A mesh dependence study has revealed that doubling the mesh density causes less than 1% change in thermal conductance.

The phonon dispersion curves of bulk silicon were reproduced and benchmarked against published data[33] to ensure the correct implementation of SW potentials. The value of δ was chosen so that thermal conductance predictions converge to within 2%. In practice, an extremely small δ can induce a high condition number for some matrices that require inversion. Two numerical benchmarks have been performed: (1) at low frequencies, the surface density of states $(-\mathrm{Im}(\mathrm{Tr}[\tilde{g}_o])/2\pi)$ is proportional to frequency ω; (2) also, at low frequencies, the transmission function exhibits a quadratic dependence on frequency.[18]

A numerical singular point exists at $\omega = 0$, which causes the denominator in phonon distribution functions $\bar{N}_L$ and $\bar{N}_R$ to be zero. A finite low-frequency integration limit ($\omega_{\mathrm{low}} = 10^{12}$ rad/s) is therefore used to numerically compute $\Delta\bar{N}$. The truncation error thus incurred can be estimated by assuming a quadratic transmission function at low frequencies[18] and evaluating the integral analytically with lower limits of ω_{low} and 0, respectively. Our estimation shows that this numerical error at 10 K is only 0.6% and is negligible at 100 K.

In recent years, more than 30 empirical potentials for silicon have been developed. Balamane *et al.*[34] concluded that the popular potentials they have tested provide a fair description of the properties of bulk silicon but fail to represent surfaces and small clusters accurately. The accuracy of the AGF method depends on the selection of interatomic potential. We have compared the results based on two different potentials [Harrison's[35] and SW (Ref. 28)] in an attempt to determine how the predicted thermal conductance depends on the selection of interatomic potential. Comparisons of

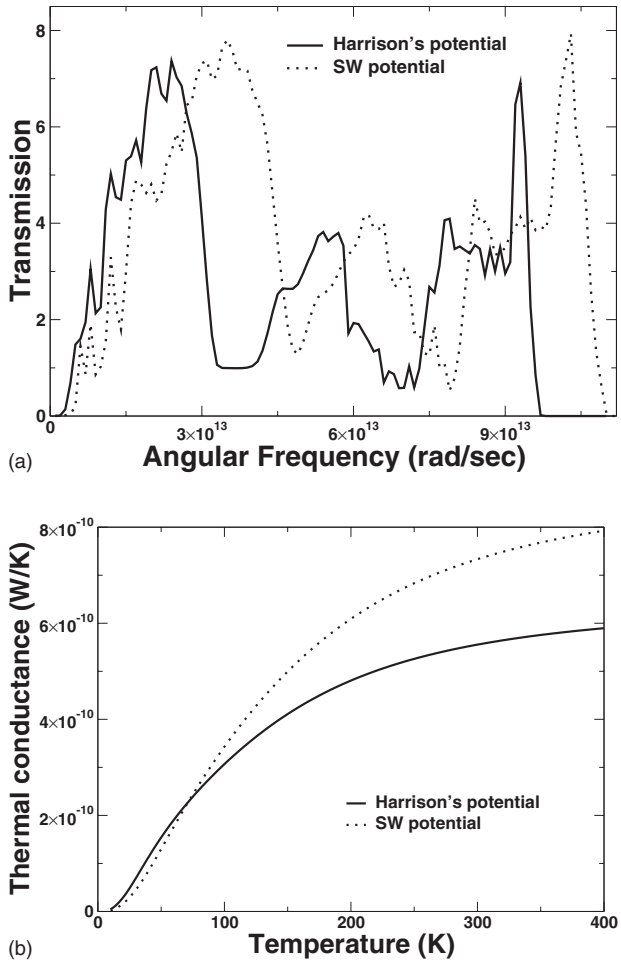

FIG. 5. Comparison of thermal conductances for Harrison's (Ref. 35) and SW potentials (Ref. 28). (a) Transmission as a function of angular frequency for different interatomic potentials. (b) Thermal conductance as a function of temperature for different interatomic potentials.

transmission and conductance are shown in Fig. 5. In this case, nine unit cells exist in the nanowire cross section, and the length of the nanowire is three unit cells.

The SW potential predicts a smaller transmission than Harrison's potential at low frequencies and generally larger transmission at higher frequencies. The SW potential also predicts an extended phonon spectrum with a 14% larger cutoff frequency. Therefore, the thermal conductance predicted by the SW potential is comparatively smaller at low temperatures and larger at high temperatures. The conductance predicted by the SW potential is within 2% of that by Harrison's potential at 10 K, while the difference grows to 30% at 300 K. It appears that the selection of interatomic potentials has a significant impact on the simulation results. However, the transmission curves of these two potentials have similar shapes, because the harmonic simplification of the SW potential results in a potential of the same form as Harrison's potential. Experimental comparisons indicate that Harrison's potential is more appropriate for cases in which a good description of the upper frequency limits of the spectrum is needed.[12] Such cases are common in nanoscale transport experiments for which boundary scattering dominates.

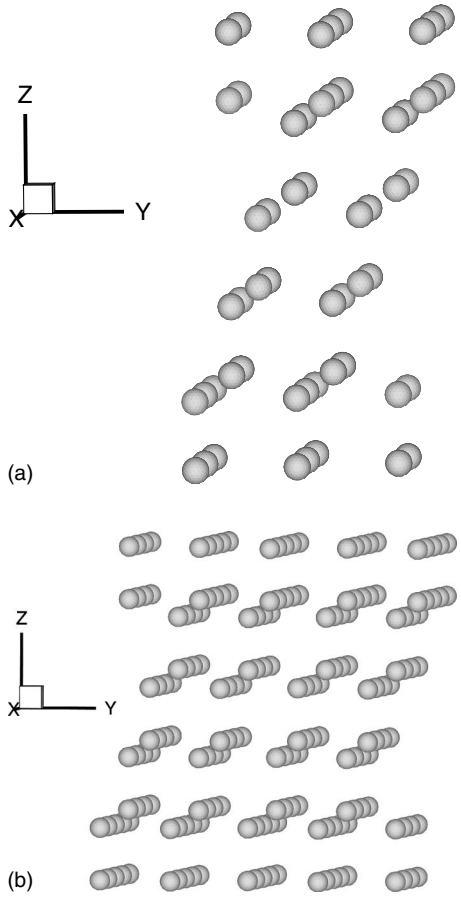

FIG. 6. LD-D-RD atoms groups with different nanowire diameters. (a) Four atoms per layer. (b) Sixteen atoms per layer.

IV. RESULTS AND DISCUSSION

A. Effects of nanowire diameter on phonon transport

A series of cases has been simulated to examine the dependence of phonon transport on nanowire diameter and its asymptotic behavior. The (111) lattice orientation is aligned with the z axis in these cases, and the length of the nanowire is three unit cells. Nanowires with different cross-sectional areas have been constructed for comparison, and two (4 unit cells and 16 unit cells per cross section) are shown in Fig. 6.

As the nanowire grows in the lateral direction, more atoms participate in thermal transport. In other words, more phonon states become available in the nanowire device, and consequently, the thermal conductance increases with increasing diameter (see Fig. 7). On the other hand, larger

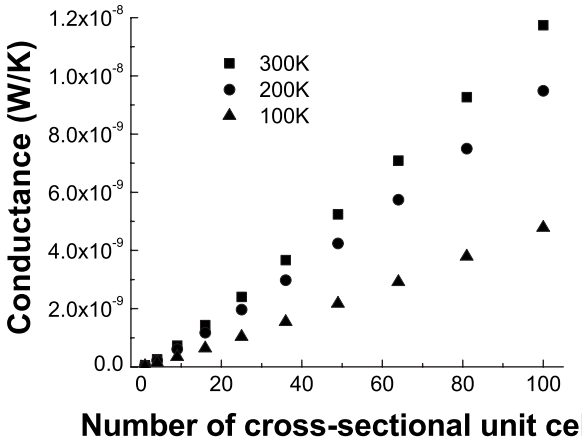

FIG. 7. Comparison of overall thermal conductance for different nanowire diameters.

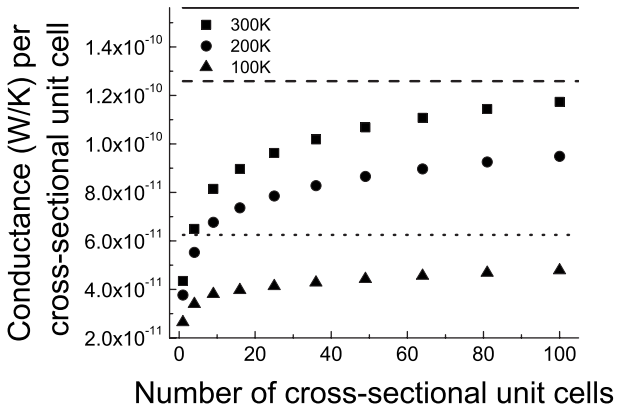

FIG. 8. Comparison of normalized thermal conductance for different nanowire diameters. Straight line: normalized thin-film conductance at 300 K; dashed line: normalized thin-film conductance at 200 K; dotted line: normalized thin-film conductance at 100 K.

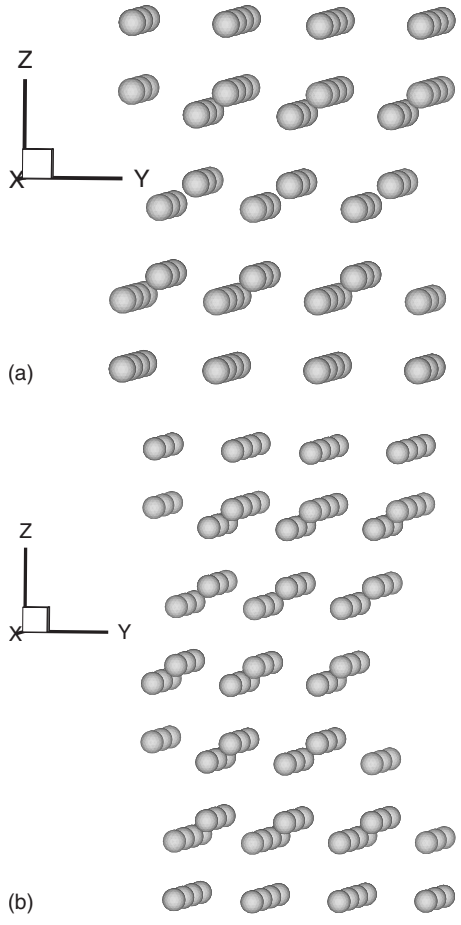

FIG. 9. LD-D-RD atoms groups with different nanowire lengths. (a) Two-unit-cell length. (b) Four-unit-cell length.

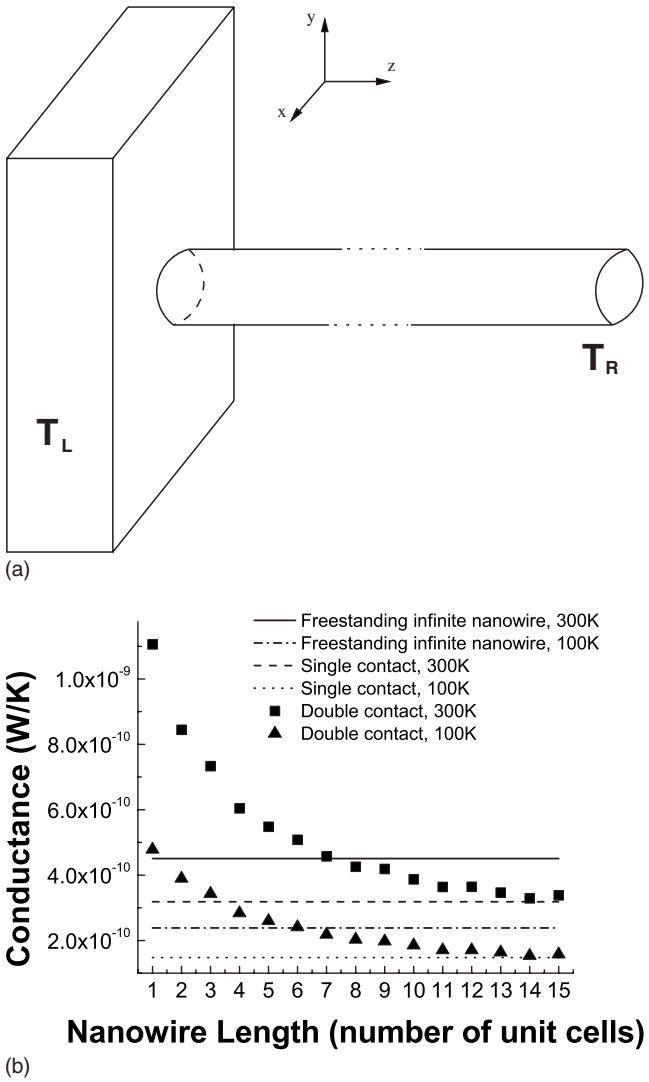

FIG. 10. Comparison of thermal conductance for different nanowire lengths and single nanowire contacts. (a) Schematic of nanowire-single-contact setup. (b) Conductance comparison.

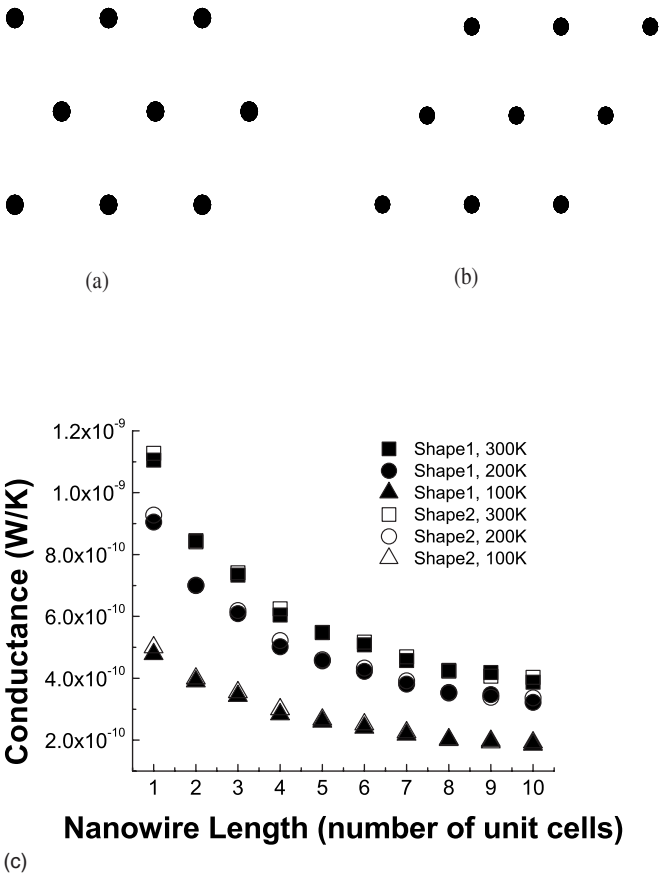

FIG. 11. Comparison of thermal conductance for different nanowire cross-sectional shapes. (a) Shape 1. (b) Shape 2. (c) Conductance comparison.

diameters also make transport in this nanowire–bulk-contact structure behave more like transport in thin films, and thus we expect the asymptotic thermal conductance per unit area in the nanowire–bulk-contact case to approach that of a thin-film case. Thermal conductance, normalized by the number of cross-section unit cells, is shown as a function of the number of unit cells per cross section in Fig. 8. Values of normalized thin-film conductances[26] at corresponding temperatures are also shown. The normalized thermal conductance in the nanowire–bulk-contact case begins to approach the asymptotic limits of the thin-film cases for the widest nanowires considered. A nanowire with a 36-unit-cell cross section (approximately 2.3 nm diameter) has a normalized conductance of 1.02×10^{-10} W/K per unit cell at 300 K (65% of the thin-film value) and 4.26×10^{-11} W/K per unit cell at 100 K (69% of the thin-film value).

B. Effects of nanowire length on phonon transport

Another series of cases has been studied to investigate the effect of nanowire length on phonon transport. Again, the (111) lattice orientation is aligned with the z axis. Nanowires with lengths of two and four unit cells are shown in Fig. 9. The cross section of the nanowires in this case consists of nine unit cells. Thermal conductance results for these cases as a function of nanowire length are shown in Fig. 10(b). Conductances at all temperatures exhibit steady decreasing trends with increasing length, primarily due to decreased coupling between reservoirs and the nanowire.[22] We have also calculated the thermal conductance of a nanowire-single-contact structure, shown in Fig. 10(a). Reference 21 explains how to use the AGF method to calculate the "infinite nanowire" case, which is a pure silicon nanowire without any bulk contact. The results show that conductances of double-contact cases can exceed those of infinite nanowires when the nanowire is very short and decrease below those of infinite nanowire cases for longer nanowires. For very long double-contacted nanowires, the thermal conductance converges to that of the single-contact case.

C. Effects of nanowire cross-section shape and orientation

One possible means of altering thermal transport is to modify the device geometry in order to affect phonon dispersion and group velocities. We have investigated the thermal conductances of two nanowires with different cross-sectional shapes, as shown in Figs. 11(a) and 11(b). The structural

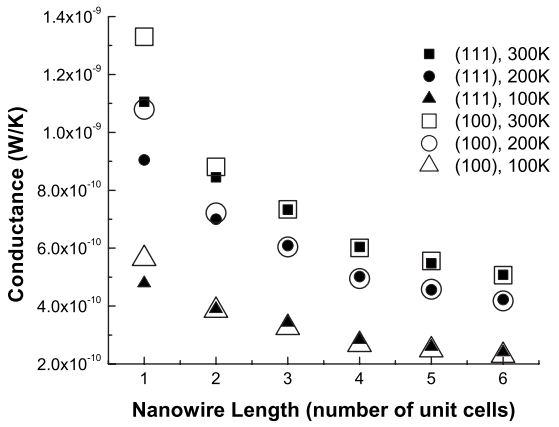

FIG. 12. Comparison of thermal conductance for different lattice orientations.

differences between these two shapes alter the harmonic matrices and transmission functions, and thus thermal conductance. The resulting conductances, integrals of transmission functions and densities of phonon subband states, are compared in Fig. 11(c). The results, however, indicate that thermal conductance appears to be insensitive to the cross-sectional shape change, as the maximum difference in the thermal conductances is less than 5%.

Another possible method is to control lattice orientation. We have investigated the thermal conductances of two nanowires with different lattice orientations, (100) and (111), aligned with the z axis. The number of cross-sectional unit cells is 9 in both cases. Because of the structural differences of these two lattices, the harmonic matrices of these two orientations differ at all nanowire lengths. Physically, the phonon subbands in the device region change as the orientation changes. Therefore, the transmission results should not be exactly the same. However, when heat conductances (as a frequency integral over all phonon subbands) are compared in Fig. 12, differences in thermal conductances are significant (15%) only in the case of a one-unit-cell length and are negligible for all other lengths,

V. SUMMARY AND CONCLUSIONS

An AGF method has been developed to simulate phonon transport across a nanowire device with bulk contacts. Bare surface Green's functions are used to calculate self-energy matrices for the abrupt interfaces between the nanowire and bulk contacts. Numerical details such as meshing of equivalent Brillouin zones have been developed. The selection of interatomic potential can greatly influence the simulation results. The dependence of phonon transport on diameter has been quantified, showing that overall conductance increases with increasing diameters, and the normalized conductance converges to the thin-film conductance. The length dependence of phonon transport has been studied and shows a steady decreasing trend for increasing nanowire length. Cross-sectional shape and lattice orientation of nanowires appear to have insignificant effects on thermal transport. The approach developed in this paper can be readily extended to study thermal transport of other nanostructure junctions, such as molecule heterojunctions and nanotubes between bulk contacts.

*Corresponding author. tsfisher@purdue.edu

[1] A. Tilke, L. Pescini, H. Lorenz, and R. Blick, Appl. Phys. Lett. **82**, 3773 (2003).
[2] C. Yung, D. Schmidt, and A. Cleland, Appl. Phys. Lett. **81**, 31 (2002).
[3] L. Shi, C. Yu, and J. Zhou, J. Phys. Chem. B **109**, 22102 (2005).
[4] S. Sinha and K. Goodson, Int. J. Multiscale Comp. Eng. **3**, 1 (2005).
[5] M. Law, J. Goldberger, and P. Yang, Annu. Rev. Mater. Sci. **34**, 83 (2004).
[6] C. Dames and G. Chen, J. Appl. Phys. **95**, 682 (2004).
[7] W.-S. Jiaung and J.-R. Ho, J. Appl. Phys. **95**, 958 (2004).
[8] Y. Chen, D. Li, J. Lukes, and A. Majumdar, J. Heat Transfer **127**, 1129 (2005).
[9] J. Callaway, Phys. Rev. **113**, 1046 (1959).
[10] M. Holland, Phys. Rev. **132**, 2461 (1963).
[11] W.-Q. Huang, K.-Q. Chen, Z. Shuai, L. Wang, and W. Hu, Int. J. Mod. Phys. B **19**, 1017 (2005).
[12] N. Mingo, Phys. Rev. B **68**, 113308 (2003).
[13] D. Li, Y. Wu, P. Kim, L. Shi, P. Yang, and A. Majumdar, Appl. Phys. Lett. **83**, 2934 (2003).
[14] D. Ferry and S. Goodnick, *Transport in Nanostructures*, 1st ed. (Cambridge University Press, Cambridge, 1997).
[15] C.-M. Chang and M. R. Geller, Phys. Rev. B **71**, 125304 (2005).
[16] M. C. Cross and R. Lifshitz, Phys. Rev. B **64**, 085324 (2001).
[17] A. Feher, A. Mamalui, A. Dul'fan, E. Syrkin, and A. Shkorbatov, Low Temp. Phys. **31**, 921 (2005).
[18] K. R. Patton and M. R. Geller, Phys. Rev. B **64**, 155320 (2001).
[19] E. P. Pokatilov, D. L. Nika, and A. A. Balandin, Superlattices Microstruct. **38**, 168 (2005).
[20] E. P. Pokatilov, D. L. Nika, and A. A. Balandin, Phys. Rev. B **72**, 113311 (2005).
[21] N. Mingo and L. Yang, Phys. Rev. B **68**, 245406 (2003).
[22] A. Buldum, S. Ciraci, and C. Fong, J. Phys.: Condens. Matter **12**, 3349 (2000).
[23] W.-X. Li, K.-Q. Chen, W. Duan, J. Wu, and B.-L. Gu, J. Phys. D **36**, 3027 (2003).
[24] Y.-M. Zhang and S.-J. Xiong, Phys. Rev. B **72**, 115305 (2005).
[25] N. Mingo, Phys. Rev. B **74**, 125402 (2006).
[26] W. Zhang, N. Mingo, and T. Fisher, J. Heat Transfer **129**, 483 (2007).
[27] W. Zhang, N. Mingo, and T. Fisher, Numer. Heat Transfer, Part B **51**, 333 (2007).
[28] F. H. Stillinger and T. A. Weber, Phys. Rev. B **31**, 5262 (1985).
[29] T. Thonhauser and G. D. Mahan, Phys. Rev. B **69**, 075213 (2004).
[30] S. Datta, *Electronic Transport in Mesoscopic Systems*, 1st ed. (Cambridge University Press, Cambridge, 1995).

[31] S. Datta, *Quantum Transport: Atom to Transistor*, 1st ed. (Cambridge University Press, Cambridge, 2005).
[32] F. Guinea, C. Tejedor, F. Flores, and E. Louis, Phys. Rev. B **28**, 4397 (1983).
[33] L. Porter, J. Justo, and S. Yip, J. Appl. Phys. **82**, 5378 (1997).
[34] H. Balamane, T. Halicioglu, and W. A. Tiller, Phys. Rev. B **46**, 2250 (1992).
[35] W. A. Harrison, *Electronic Structure and the Properties of Solids* (Dover, New York, 1989).